J. Astron. Space Sci. 15(1), 27–38 (1998)

ON THE EXTRACTION OF OPTICAL ROTATION CURVES FOR SPIRAL GALAXIES

Young-Jong Sohn[1], Myung-Hyun Rhee[1], and Mun-Suk Chun[2]
[1]Center for Space Astrophysics, Yonsei University, Seoul 120-749, Korea
[2]Department of Astronomy, Yonsei University, Seoul 120-749, Korea
e-mail: sohnyj@csa.yonsei.ac.kr

(Received May 6, 1998; Accepted May 25, 1998)

ABSTRACT

We discussed four different methods - the single, double and triple Gaussian fits, and the intensity weighted centroid fit - which extract rotation curves from several emission lines (*i.e.* [OII], Hβ, [OIII], and Hα) of spiral galaxies. Spatial extents and the shapes of rotation curves derived through various methods applying to each emission lines of a sample galaxy UGC 11635 are all in a good agreement with one another. Linewidths of Hβ and Hα measured from rotation profiles are in a good agreement with Hα linewidth of Courteau (1992). However, linewidths of [OII] seems to be much broader than Hα, and the profile of [OIII] does not follow the profile of Hα.

1. INTRODUCTION

The Tully-Fisher relation (Tully & Fisher 1977, hereafter TF), which has become one of the most powerful and widely used tools for studying cosmic velocity fields in the local universe (Strauss & Willick 1995, Rhee 1996 for a review), is an empirical correlation between some suitably defined measures of the peak rotational velocity (or the linewidth) of a galaxy and the total absolute magnitude. The basic physical interpretation of the empirical TF relation is that the profile width gives an estimate of the total mass, which in terms is directly correlated to the total light of the galaxy.

Measurements of TF rotational velocities have primarily relied on single radio observation of neutral hydrogen at 21 cm. However, HI TF method is limited by the sensitivity of current radio telescope to $z < 0.1$. Therefore, emission lines traced in the optical domain provide a most adequate substitute to 21 cm emission. Because of their high luminosity and easy spectroscopic accessibility, HII region emission line of Hα 6563 Å is mostly often used in study of galaxy rotation at low-z, and the good match between radio and optical velocity widths of Hα has been verified by Courteau (1997, 1992), Mathewson *et al.* (1992), Dressler & Faber (1990), and Courteau & Faber (1988). However, Hα observation is limited by the fact that Hα is redshifted out of the optical bandpass for distant galaxies with $z > 0.4$. So, until IR spectrometers become available, line widths of distant spiral galaxies will have to be measured using blue optical emission lines, such as [OII] 3726.2 +

3728.9 Å, Hβ 4861 Å, and [OIII] 4959, 5007 Å. Vogt *et al.* (1993, 1996, 1997) show rotation curves for 12 galaxies from blue emission lines at $0.15 < z < 0.75$. Forbes *et al.* (1996) measured velocity widths of blue emission lines for a sample of 18 galaxies with redshifts $0.2 < z < 0.84$. We note that HII region spectra show some other emission lines through optically blue wavelength region, such as Hγ, Hδ, Hη, and [Ne III] lines. However, line intensities for these emissions are usually too weak to be used on the rotation curve studies for external galaxies, compared to those of blue emission lines used in this paper (cf. Zaritsky *et al.* 1994).

Various techniques have been introduced independently to extract the rotation velocities from each optical emission lines. Because of its doublet feature, double Gaussian fit has been usually applied to extract a rotation curve for the [OII] line (Vogt *et al.* 1993, 1996, 1997). Raychaudhury *et al.* (1997) used the triple Gaussian profiles to fit the Hα and two adjacent [NII] emission lines. On the other hand, Courteau (1997) measured the intensity weighted centroids at each row along the Hα galaxy emission using a parabolic binned interpolation technique.

The purpose of this paper is to do intercomparison of optical rotation curves for blue emission lines and Hα, which were extracted by various methods, and line profile widths of each emission lines in a galaxy sample. We applied then all of four techniques - single, double, and triple Gaussian fits and intensity weighted centroid fit - to extract rotaion velocities from long slit spectra of [OII], Hβ, [OIII], and Hα emission lines of a sample galaxy UGC 11635 ($v_r = 4812 kms^{-1}$). In Section 2, we describe the long-slit spectral data of UGC 11635 and data reductions. The extraction of rotation curves from resolved emission lines is discussed in Section 3. Linewidths derived from the rotaion profiles of each emission lines are also discussed in Section 4. The summary of results is given in Section 5.

2. SAMPLE SPECTRA AND DATA REDUCTIONS

We use the long-slit spectra of UGC 11635 as a sample galaxy, which consist of [OII] doublet, Hβ, [OIII] 5007 Å, and Hα emission lines. Spectroscopic observations for the galaxy were made at September 21, 1995 using the Kast spectrograph on Shane 3 m telescope at UCO/Lick observatory by Courteau (private communication). Kast spectrograph consists of two separated spectrographs, housed in a single structure - one optimized for red (3800 - 7300 Å) and the other for blue (3200 - 4550 Å). Dichroic beamsplitters and two 1200 × 400 UV flooded Reticon detectors allow simultaneous observations in red and blue. [OII] doublet has been recorded in the blue camera, while the [OIII] and Hβ lines have been observed in the red camera. Hα emission spectrum was obtained separately on the other observing run. The gain and readout noise are 3.8e-/DN and 6e-, respectively. Image scale is 0.798 arcsec/pixel. Average FWHM of spectral lines is about 2.2 Å, which is estimated from a few strong sky lines. The slit was aligned to the galaxy's major axis during the observation.

Pixel-to-pixel variations were removed by subtraction of a constant bias level and division with flat-fileds generated from dome-flat images. Flat field errors are estimated $\sim 2\%$ in blue and $\sim 4\%$ in red wavelength regions relative to 20,000DN. Twilight exposures were used to compensate the illumination effect dependent on the position of the slit. The line curvature was mapped from the calibration spectra whereas S-distortion mapping was modeled directly from the galaxy's continuum. A polynomial pixel-wavelength fit was extracted from each He-Hg-Cd calibration spectrum using

Table 1. Optical rotation velocities of [OII] for UGC 11635.

R(″)	V(kms^{-1})	σ_V	R(″)	V(kms^{-1})	σ_V	R(″)	V(kms^{-1})	σ_V
-50.5	-271.3	12.0	-2.9	-116.9	12.4	14.2	199.9	16.7
-48.2	-211.6	30.5	-2.1	-32.3	20.3	15.0	207.0	14.1
-43.5	-279.2	14.4	-1.4	-69.5	7.9	16.6	258.5	18.9
-42.7	-252.0	22.1	1.0	63.5	10.6	17.4	211.5	5.8
-41.9	-210.3	22.2	1.8	189.5	24.3	22.8	176.7	26.9
-39.6	-279.7	19.0	2.5	85.6	4.4	26.7	180.4	14.1
-30.2	-202.3	21.5	7.2	249.6	24.8	29.1	195.4	26.9
-12.3	-260.4	26.9	8.0	211.1	23.0			
-11.5	-262.3	8.5	13.5	252.1	10.4			

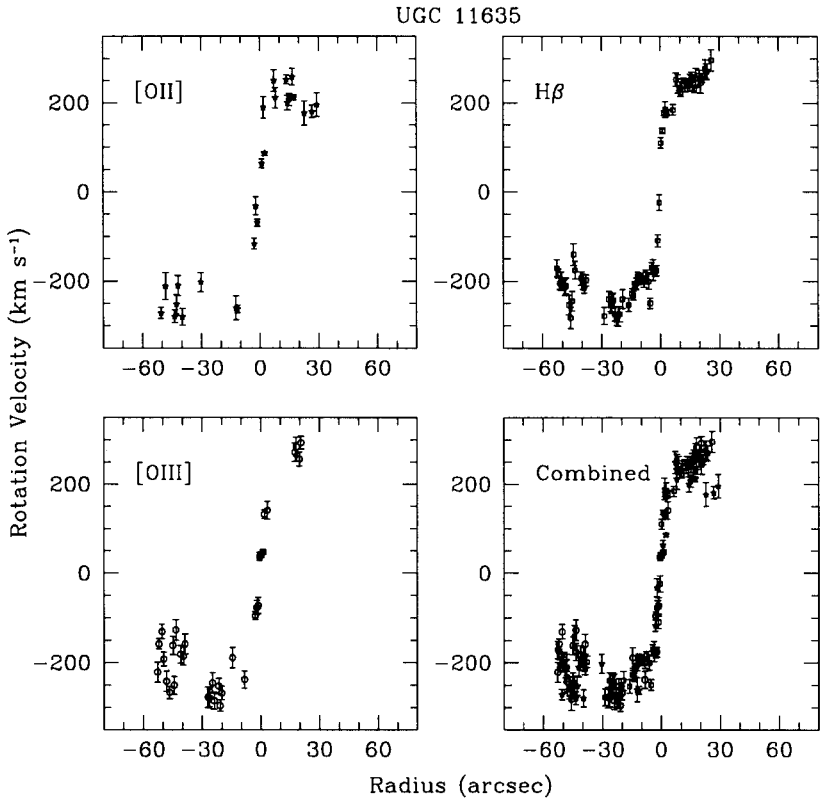

Figure 1. Optical rotation curves of UGC 11635 derived from blue emission lines [OII], Hβ, and [OIII].

Table 2. Optical rotation velocities of Hβ for UGC 11635.

R(″)	V(kms^{-1})	σ_V	R(″)	V(kms^{-1})	σ_V	R(″)	V(kms^{-1})	σ_V
-52.7	-171.3	18.9	-20.8	-273.7	17.7	2.6	185.2	17.5
-52.0	-182.8	9.8	-19.2	-240.2	21.4	3.4	178.1	7.9
-51.2	-205.1	13.9	-16.1	-252.9	15.1	6.5	184.1	11.8
-50.4	-200.1	20.3	-14.5	-227.4	10.6	8.1	252.1	15.6
-48.8	-214.2	18.5	-13.7	-231.8	9.8	8.9	242.5	20.7
-48.1	-210.5	17.6	-13.0	-209.0	7.6	9.7	233.3	6.0
-46.5	-252.7	21.9	-12.2	-206.0	12.6	10.4	223.0	8.6
-45.7	-282.3	24.1	-11.4	-189.2	9.2	11.2	239.5	14.1
-44.9	-244.5	21.7	-10.6	-191.3	9.2	12.0	250.1	6.3
-44.2	-140.6	24.1	-9.8	-198.8	7.9	12.8	229.0	3.9
-43.4	-175.4	19.3	-8.3	-200.4	12.6	13.6	245.6	8.4
-40.3	-193.7	15.1	-7.5	-184.0	9.3	14.3	242.5	7.6
-39.5	-201.3	17.0	-5.9	-200.8	16.6	15.1	245.4	18.9
-38.7	-214.8	12.3	-5.2	-249.4	12.2	15.9	258.3	11.4
-37.9	-198.2	12.7	-4.4	-170.2	11.2	16.7	251.2	12.4
-28.6	-277.3	18.9	-3.6	-174.9	23.1	17.5	231.3	8.3
-26.2	-240.1	17.7	-2.8	-178.0	10.3	18.2	255.8	21.3
-25.4	-251.4	16.5	-2.0	-176.3	11.1	19.8	262.0	12.4
-24.7	-250.7	21.4	-1.3	-109.5	13.9	20.6	244.6	22.3
-23.9	-243.0	17.5	-0.5	-23.9	17.9	21.4	255.1	10.1
-23.1	-273.2	16.1	0.3	109.8	11.3	22.9	276.9	21.2
-22.3	-285.6	13.2	1.1	137.0	5.8	23.7	270.3	17.3
-21.5	-277.9	22.5	1.9	177.1	5.2	26.0	295.8	23.8

Table 3. Optical rotation velocities of [OIII] for UGC 11635.

R(″)	V(kms^{-1})	σ_V	R(″)	V(kms^{-1})	σ_V	R(″)	V(kms^{-1})	σ_V
-52.7	-221.2	22.7	-38.7	-158.2	22.5	-2.0	-76.8	15.4
-52.0	-158.5	11.2	-27.0	-277.7	23.3	-1.3	-73.0	17.7
-50.4	-130.3	16.3	-26.2	-279.3	19.7	-0.5	37.1	8.7
-49.6	-192.0	15.1	-24.7	-245.5	23.4	0.3	41.1	6.7
-48.1	-242.1	23.1	-23.9	-285.5	19.4	1.1	47.2	5.4
-46.5	-266.9	13.7	-21.5	-252.7	17.7	1.9	131.6	9.3
-44.9	-161.2	20.3	-20.8	-296.2	12.6	3.4	140.7	19.7
-44.2	-251.1	20.3	-20.0	-268.0	15.5	17.5	272.0	21.0
-43.4	-126.7	23.0	-14.5	-188.7	22.7	18.2	284.4	21.4
-41.0	-181.4	19.4	-8.3	-238.2	19.1	19.8	256.5	15.8
-39.5	-185.5	20.3	-2.8	-95.0	9.4	20.6	293.2	14.5

interactive line identification. Line flexure through the spectra has been corrected with 5 or more unblended bright sky lines. Sky backgrounds were subtracted by interpolating with a second-order polynomial to the background rows above and below the galaxy emission. Cosmetic defect corrections and cosmic rays removal were also performed interactively. Last, galaxy continuum or all the uniform structure parallel to the dispersion axis has been removed by row-by-row background polynomial fit.

3. EXTRACTION OF THE ROTATION VELOCITIES

Best-fit of double Gaussian fit to the [OII] doublet, with rest frame centers fixed at 3726.2 Åand 3728.9 Å, derives the positions, amplitude, width, and a linear background of the emission line. Using the two peak positions of [OII] doublet, we estimated the radial velocities at each positions of

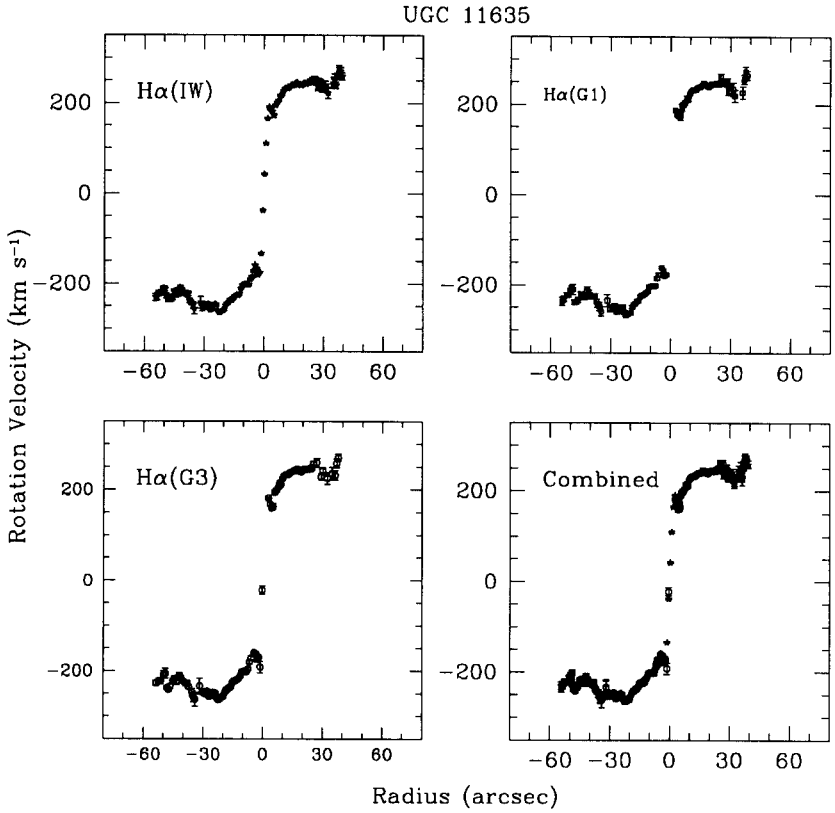

Figure 2. Hα optical rotation curves of UGC 11635 derived from methods of the intensity weighted centroid fit (IW), the single Gaussian fit (G1), and the triple Gaussian fit (G3).

spatial axis. Table 1 lists rotation velocities extracted from [OII] doublet using the double Gaussian fit.

For the [OIII] and Hβ emission lines, we applied the intensity weighted centroid fit to extract rotation velocities. The emission line centroid is given by

$$< x >= \frac{\Sigma_i (x_i - x_0) f_i}{\Sigma_i f_i} = \Sigma_i (x_i - x_0) w_i$$

where we have defined the pixel weights, a,

$$w_i = \frac{f_i}{\Sigma_i f_i} = \frac{f_i}{F},$$

and where F is the total flux under the curve. The error of the centroid is given by

Table 4. Optical rotation velocities of Hα for UGC 11635 derived from the intensity weighted centroid fit.

R(″)	V(kms^{-1})	σ_V	R(″)	V(kms^{-1})	σ_V	R(″)	V(kms^{-1})	σ_V
-54.2	-230.7	7.8	-21.5	-262.7	1.7	8.9	216.5	1.5
-53.5	-231.5	5.4	-20.7	-259.8	2.2	9.7	225.8	1.3
-52.7	-221.4	5.4	-19.9	-258.0	2.5	10.5	231.6	1.2
-51.9	-222.6	5.1	-19.1	-248.5	2.1	11.3	232.5	1.1
-51.1	-221.2	3.2	-18.4	-244.0	2.3	12.1	232.2	1.1
-50.3	-212.1	5.2	-17.6	-241.8	2.8	12.8	234.2	1.2
-49.6	-212.1	5.2	-16.8	-236.1	3.1	13.6	239.1	1.4
-48.8	-227.1	5.8	-16.0	-236.1	2.8	14.4	239.6	1.8
-48.0	-236.8	4.5	-15.2	-231.6	2.7	15.2	239.6	2.2
-47.2	-236.6	4.2	-14.5	-228.3	2.2	16.0	244.1	2.3
-46.4	-234.6	4.8	-13.7	-225.7	1.9	16.7	245.2	2.4
-45.7	-231.1	5.6	-12.9	-226.6	1.8	17.5	241.1	2.8
-44.9	-218.8	5.5	-12.1	-223.3	1.9	18.3	239.7	3.0
-44.1	-224.4	6.6	-11.3	-211.5	1.2	19.1	239.5	2.5
-43.3	-218.2	8.2	-10.6	-203.4	1.5	19.9	242.4	2.3
-42.5	-224.0	5.0	-9.8	-202.1	1.6	20.6	243.8	2.3
-41.8	-209.7	4.6	-9.0	-202.5	1.5	21.4	241.6	2.7
-41.0	-213.5	3.0	-8.2	-203.1	1.7	22.2	245.8	2.8
-40.2	-220.6	2.3	-7.4	-202.4	2.0	23.0	249.6	2.9
-39.4	-221.3	2.5	-6.7	-190.6	2.7	23.8	246.2	3.7
-38.6	-225.2	3.7	-5.9	-185.5	3.2	24.5	244.6	4.7
-37.9	-222.6	5.4	-5.1	-172.1	2.9	25.3	252.7	6.6
-37.1	-238.7	4.8	-4.3	-158.7	1.5	26.1	248.8	8.1
-36.3	-242.7	4.7	-3.5	-166.9	1.2	26.9	236.3	8.9
-35.5	-248.4	7.4	-2.8	-180.5	0.9	27.7	246.8	7.1
-34.7	-255.8	11.7	-2.0	-175.8	1.3	28.4	243.1	8.8
-31.6	-242.4	13.2	-1.2	-133.6	1.8	29.2	229.6	5.3
-30.8	-250.3	10.4	-0.4	-37.7	2.0	30.0	239.0	9.9
-30.1	-250.6	6.1	0.4	42.7	1.6	30.8	237.2	11.0
-29.3	-252.6	4.5	1.1	110.2	1.7	31.6	232.1	10.0
-28.5	-247.8	3.9	1.9	165.3	1.5	32.3	222.4	12.1
-27.7	-245.9	3.5	2.7	190.6	1.4	34.7	244.3	12.4
-26.9	-258.2	2.3	3.5	185.6	2.4	35.5	251.0	12.9
-26.2	-257.1	2.0	4.3	180.4	3.4	36.2	238.8	7.7
-25.4	-249.3	2.2	5.0	171.8	4.0	37.0	259.5	6.2
-24.6	-246.6	2.9	5.8	194.7	2.7	37.8	276.2	6.0
-23.8	-247.3	3.3	6.6	200.6	2.6	38.6	269.7	9.2
-23.0	-259.5	2.1	7.4	205.8	1.8	39.4	258.9	8.3
-22.3	-264.2	1.6	8.2	216.1	1.7			

$$\sigma^2 < x >= \Sigma_i (x_i - x_0)^2 \sigma^2_{w_i} + \Sigma_{i,j} (x_i - x_0)(x_j - x_0)\sigma_{w_i w_j}.$$

Table 2 and Table 3 list the derived rotation velocities from Hβ and [OIII] emissions using the intensity weighted centroid fit. Figure 1 shows the rotation curves derived from each emission lines indicating very similar shapes each other. Moreover, spatial extents of each rotation curves are very similar, too, *i.e.* 50.5″ for [OII], 52.7″ for Hβ and [OIII].

Hα emission line in spiral galaxies has two adjacent [NII] emission lines. A typical normal spiral galaxy nuclear template has relative intensities for the emission lines of Hα and [NII] 6548, 6583 Å with Hα strongest and [NII] 6548 Å weakest, even though many spiral galaxies show the nuclear Hα/[NII] reversal (Strochi-Bergmann 1991, Rubin & Ford 1986). Therefore, we applied three different methods to extract the rotaion curves from Hα emission line, *i.e.* the triple Gaussian fit to Hα and [NII]s, the single Gaussian fit and the intensity weighted centroid fit to the Hα only.

Table 5. Optical rotation velocities of Hα for UGC 11635 derived from the single Gaussian fit.

R(″)	V(kms^{-1})	σ_V	R(″)	V(kms^{-1})	σ_V	R(″)	V(kms^{-1})	σ_V
-54.2	-236.0	8.9	-23.0	-261.2	2.9	8.2	215.1	3.2
-53.5	-231.3	6.5	-22.3	-266.8	2.6	8.9	211.1	3.0
-51.9	-222.2	4.7	-21.5	-265.1	2.9	9.7	223.5	2.3
-51.1	-222.9	5.3	-20.7	-262.0	3.3	10.5	229.9	1.8
-50.3	-214.2	6.4	-19.9	-261.3	3.7	11.3	231.9	1.7
-49.6	-208.7	6.8	-19.1	-248.7	3.0	12.1	231.9	1.7
-48.8	-210.7	11.4	-18.4	-243.6	3.0	12.8	233.4	1.8
-48.0	-238.4	5.0	-17.6	-241.2	3.6	13.6	237.3	2.0
-47.2	-237.7	4.1	-16.8	-236.6	3.5	14.4	239.7	2.4
-46.4	-233.5	5.4	-16.0	-235.2	3.4	15.2	239.7	2.7
-44.9	-221.4	5.9	-15.2	-225.9	3.3	16.0	242.7	2.7
-44.1	-224.3	7.6	-14.5	-223.5	2.7	16.7	246.9	2.9
-43.3	-224.5	7.6	-13.7	-222.8	2.2	17.5	243.7	3.4
-42.5	-224.6	6.2	-12.9	-220.4	2.3	18.3	243.2	4.3
-41.8	-212.3	9.0	-12.1	-217.2	2.4	19.1	239.3	3.6
-41.0	-216.9	5.5	-11.3	-213.4	2.5	19.9	242.2	2.9
-40.2	-222.9	3.3	-10.6	-204.0	2.7	20.6	245.4	3.1
-39.4	-226.4	3.2	-9.8	-203.2	3.1	21.4	243.4	3.2
-38.6	-224.8	3.6	-9.0	-201.8	2.7	22.2	246.3	3.2
-37.9	-225.4	5.5	-8.2	-203.1	3.0	23.0	247.0	3.8
-37.1	-236.3	4.9	-7.4	-201.1	3.3	23.8	243.9	4.6
-36.3	-243.8	5.3	-6.7	-185.0	4.2	24.5	247.3	5.5
-35.5	-247.3	9.2	-5.9	-177.6	4.4	25.3	260.7	7.3
-34.7	-258.1	10.4	-4.3	-161.5	3.0	26.1	252.0	6.0
-31.6	-234.5	14.3	-3.5	-168.0	3.0	27.7	249.2	8.2
-30.1	-251.7	7.1	-2.8	-179.3	2.2	28.4	248.9	9.1
-29.3	-254.2	4.9	-2.0	-176.7	2.0	29.2	228.5	7.3
-28.5	-248.5	4.8	2.7	187.0	2.4	30.0	239.5	6.8
-27.7	-245.9	4.6	3.5	178.0	4.1	31.6	233.5	15.1
-26.9	-259.9	3.4	4.3	176.6	7.2	32.3	219.4	13.6
-26.2	-258.9	3.0	5.0	174.6	9.3	36.2	226.5	13.8
-25.4	-251.1	3.2	5.8	194.1	7.3	37.0	255.6	9.9
-24.6	-247.9	4.2	6.6	199.7	5.1	37.8	272.8	10.7
-23.8	-248.3	4.7	7.4	203.8	3.8	38.6	264.4	9.7

For the triple Gaussian fit with a linear background, the spectral model has two parameters for continuum, six line strengths and width parameters, and one velocity parameter. Typical error threshold limit for the estimated velocities is 0.3 pixel, which leads to the velocity uncertainties smaller than 30 kms^{-1}. Table 4, Table 5, and Table 6 list the extracted Hα rotation velocities from the intensity weighted centroid methods, the single Gaussian fit, and the triple Gaussian fit. Figure 2 is the intercomparison of each rotaion curves of Hα, which shows a good match each other. Spatial extents of Hα rotation curves are estimated 54.2″ from the intensity weighted centroid fit and the single Gaussian fit, and 53.5″ from the triple Gaussian fit.

In Figure 3, we show all of the derived rotation curves from each emission lines with the Hα rotation curve of Courteau (1992), who estimated the spatial extent of Hα for UGC 11635 as 53.6″. Indeed, spatial extents and the shapes of rotation curves derived in this paper through various methods are all in good agreements with the results of Courteau (1992). Note that rotation curves extracted from blue emission lines in this paper show somewhat larger scatters probably due to their lower S/N ratios.

Table 6. Optical rotation velocities of Hα for UGC 11635 derived from the triple Gaussian fit.

R(″)	V(kms^{-1})	σ_V	R(″)	V(kms^{-1})	σ_V	R(″)	V(kms^{-1})	σ_V
-53.5	-227.4	6.2	-21.5	-262.6	2.4	7.4	203.4	3.2
-51.9	-222.6	4.7	-20.7	-258.5	3.0	8.2	213.7	2.7
-51.1	-223.3	5.1	-19.9	-257.5	3.0	8.9	210.3	2.5
-49.6	-208.0	6.6	-19.1	-249.6	2.5	9.7	223.8	2.0
-48.8	-206.3	10.9	-18.4	-242.3	2.6	10.5	230.3	1.6
-48.0	-237.9	4.8	-17.6	-242.2	3.0	11.3	232.1	1.5
-47.2	-242.1	4.4	-16.8	-237.2	2.8	12.1	231.9	1.5
-46.4	-234.8	5.4	-16.0	-236.7	3.2	12.8	233.2	1.6
-44.9	-222.6	5.4	-15.2	-226.8	2.8	13.6	237.0	1.8
-44.1	-217.6	6.0	-14.5	-223.5	2.2	14.4	239.0	2.0
-43.3	-224.6	6.9	-13.7	-222.7	2.0	15.2	240.8	2.4
-41.8	-211.6	7.0	-12.9	-220.5	1.9	16.0	240.8	2.4
-41.0	-215.6	4.7	-12.1	-218.1	2.1	16.7	244.0	2.5
-40.2	-221.7	3.0	-11.3	-212.4	2.2	17.5	243.8	3.1
-39.4	-224.8	2.9	-10.6	-203.4	2.3	18.3	242.1	3.5
-38.6	-228.9	3.8	-9.8	-202.2	2.8	19.1	238.7	3.0
-37.9	-227.9	5.1	-9.0	-201.6	2.4	19.9	242.2	2.5
-37.1	-235.7	4.4	-8.2	-203.1	2.6	20.6	245.3	2.6
-35.5	-248.1	8.1	-7.4	-196.9	3.1	21.4	243.5	2.6
-34.7	-258.9	10.3	-6.7	-181.3	3.6	22.2	245.2	2.7
-34.0	-263.3	15.2	-5.9	-172.5	3.7	23.0	245.2	3.1
-31.6	-234.0	17.0	-4.3	-159.7	2.6	23.8	244.9	3.5
-30.1	-247.0	6.2	-3.5	-162.8	2.7	24.5	248.1	5.2
-29.3	-250.5	4.2	-2.8	-175.1	2.0	25.3	255.6	6.6
-28.5	-251.6	4.0	-2.0	-170.4	2.0	26.9	258.8	9.7
-27.7	-245.3	3.9	-1.2	-192.6	12.7	29.2	228.2	7.3
-26.9	-257.6	2.8	-0.4	-21.6	9.0	30.0	241.5	6.7
-26.2	-255.6	2.3	2.7	180.9	2.1	32.3	224.4	12.7
-25.4	-249.8	2.5	3.5	167.7	3.6	34.7	235.1	14.0
-24.6	-248.3	3.4	4.3	158.8	5.2	36.2	230.7	10.7
-23.8	-249.6	4.0	5.0	162.1	6.4	37.0	257.3	9.5
-23.0	-260.9	2.5	5.8	193.8	5.4	37.8	270.1	7.9
-22.3	-264.8	2.1	6.6	197.3	4.6			

4. ROTATION PROFILES OF EMISSION LINES

With resolved optical spectra, we can measure not only rotation curves but rotation profiles, too. The optical rotation profile is a mesh of all the velocity channels along the spatial axis of the galaxy.

Figure 4 shows the rotation profiles of each emission lines for UGC 11635. A base line of the profile was subtracted by fitting a straight line to the three continuum points on each side of the edge of the profile. These edges were determined by finding the first minimum on each side of the profile. They are marked by vertical arrows in Figure 4. After subtracting the baseline, we measured the total area under the profile inside the minima. This area is measured by integrating along the velocity axis and using parabolic binned interpolation at each channel. The rotation profiles are then normalized to the total area and compared to the normalized rotation profile of Courteau (1992). Hα and Hβ profiles show a good match to the Hα rotation profile of Courteau (1992). However, in the case of [OII], the rotation profile seems to be much broader than Hα, because [OII] line is a doublet of two transitions. Line profile of [OIII] also does not follow the profile of Hα because of its low S/N ratio.

Using these rotation profiles, we measured velocity widths, W20, which is defined as the velocity separation between the two velocities where the integrated area cumulates to 10% and 90% of the total area. Results are shown in Table 7. Velocity widths of Hβ, [OIII] and Hα are in agreement with

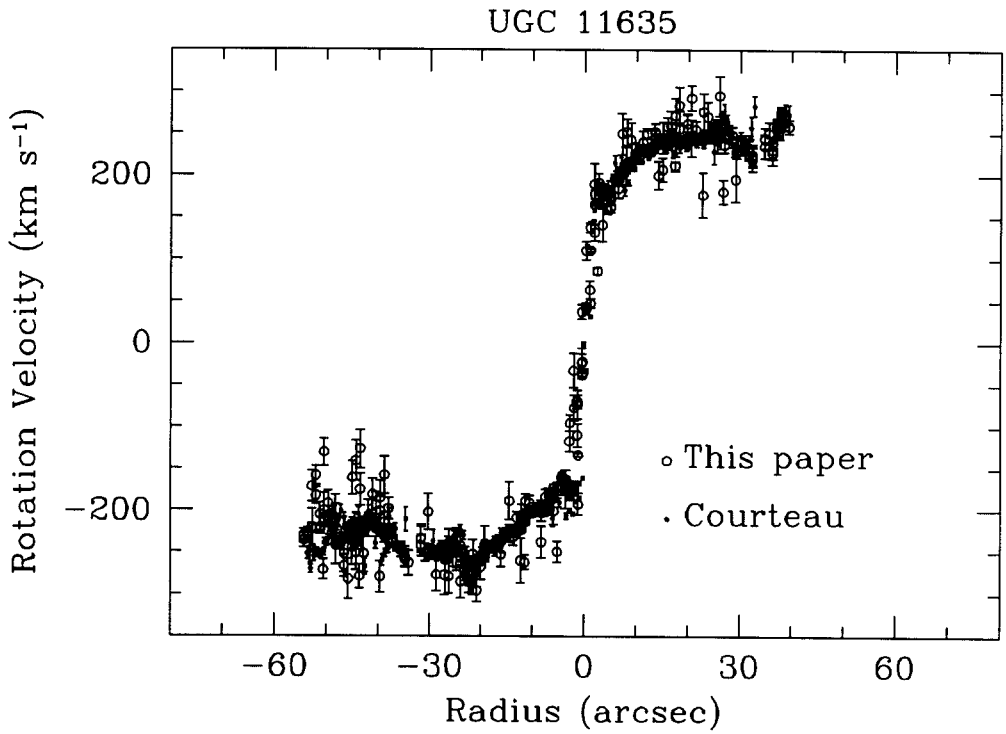

Figure 3. Optical rotaion curves of UGC 11635. Open circles are the reseults of this paper, while small dots represent the Hα rotation velocities of Courteau (1992).

W20 of Hα of Courteau (1992). But, W20 for [OII] line still has a larger value of linewidth because of its doublet feature. The radial distribution of [OII] and [OIII] will depend on the abundance and temperature of the HII regions in a complicated way compared to Hα (Zaritsky *et al.* 1994). Moreover, some uncertainties still remain regarding the shape of these blue emission lines profiles, as they are affected by dust absorption much more severely than Hα. Prada *et al.* (1994) found that differences in velocities at different wavelengths due to the effect of extinctions. McKeith *et al.* (1993) also showed that the longer the observing wavelength, the larger the velocity gradient in the optical rotation curves. Therefore, to extract rotation profiles or linewidths from [OII] and [OIII] emission lines (or even Hβ line), a careful calibration will be necessary considering to the spatial dust distributions and the abundance of HII regions in spiral galaxies.

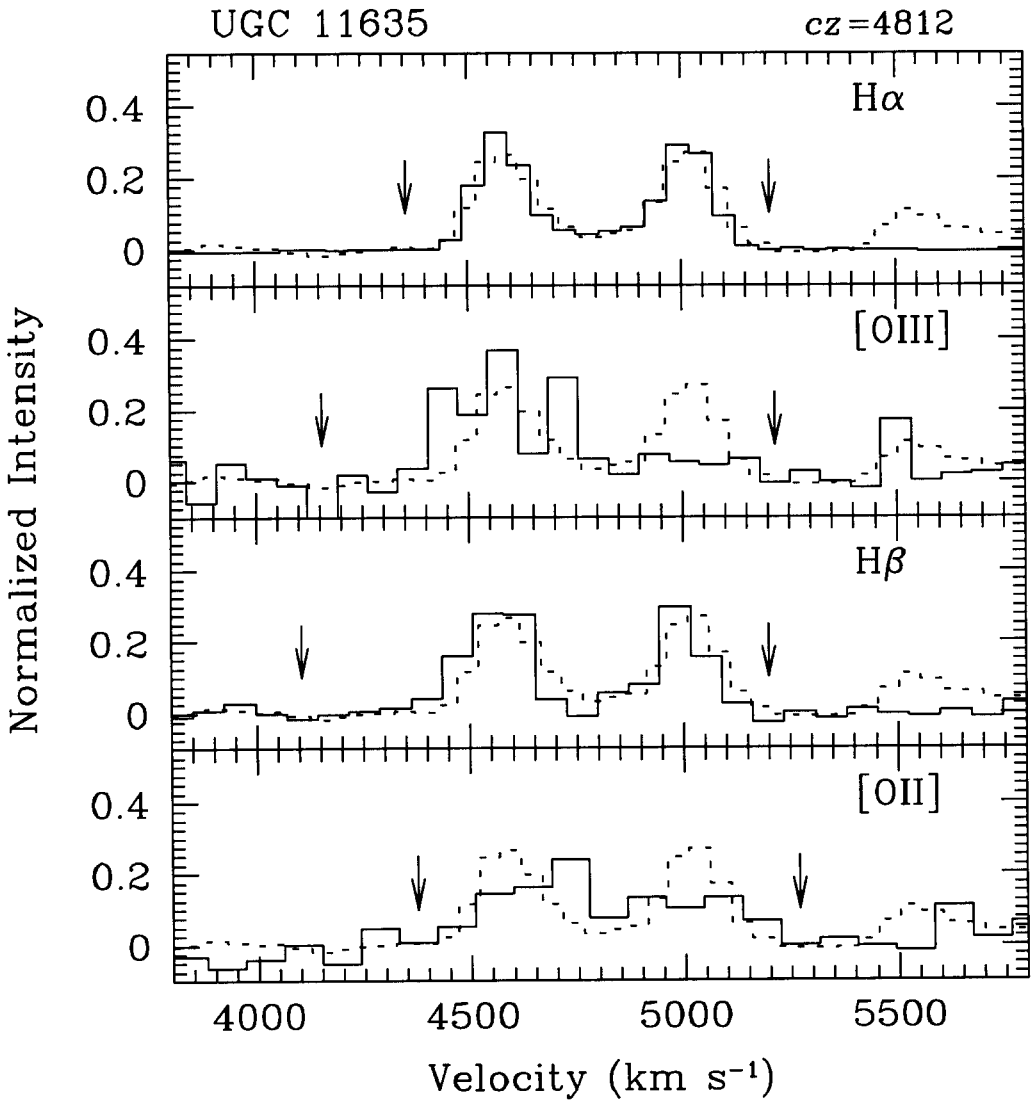

Figure 4. Emission line profiles (*solid histogram*) of UGC 11635 compared to the Hα profile (*dotted histogram*) of Courteau (1992).

Table 7. Velocity widths of emission lines for UGC 11635.

Lines	W20 (kms^{-1})
[OII]	558.2
Hβ	539.0
[OIII]	522.4
Hα	518.6
Hα[1]	523.9

[1] Courteau (1992)

5. SUMMARY

Four different methods, extracting rotation curves from several emission lines ([OII], Hβ, [OIII], and Hα) of a galaxy, have been discussed to do intercomparison of the shapes of each rotation curves. While the double Gaussian fit has been applied to the [OII] doublet, the intensity weighted centroid fit has been used to extract the rotation curves from Hβ and [OIII] emission lines. For the Hα emission, which has two adjacent [NII] emissions, we applied three different methods to extract the rotation curve, i.e. the single and triple Gaussian fit, and the intensity weighted centroid fit. Spatial extents and the shapes of rotation curves derived through various methods are all in a good agreement with one another. From the optical rotation profiles, we also estimated the linewidths (W20) of each emission lines. While linewidths of Hβ and Hα are in a good agreement with Hα linewidth of Courteau (1992), the rotation profile of [OII] seems to be much broader than Hα. Line profile of [OIII] also does not follow the profile of Hα. After careful intercomparisons of rotation curves and line profiles extracted from blue emission lines with various methods, we conclude that blue emission lines can be used to obtain rotation curves for intermediate-redshifte galaxies. We also conclude that one should be very careful for using linewidths of blue emission lines as rotation parameter for the Tully-Fisher relation.

ACKNOWLEDGEMENTS: Sincere thanks are extended to the anonymous refree for suggesting many improvements. This paper is supported by Creative Research Initiatives of the Korean Ministry of Science and Technology.

REFERENCES

Courteau, S. 1992, Ph.D. thesis, University of California, Santa Cruz
Courteau, S. 1997, AJ, 114, 2402
Courteau, S. & Faber, S. M. 1988, in The Extragalactic Distance Scale, eds. S. van den Bergh & C. Pritchet (ASP: San Fransisco), p.366
Dressler, A. & Faber, S. M. 1990, ApJ, 354, 45
Forbes, D. A., Phillips, A. C., Koo, D. C. & Illingworth, G. 1996, ApJ, 462, 89
Mathewson, D. S., Ford, V. L. & Buchhorn, M. 1992, ApJS, 81, 413
McKeith, C. D., Castle, J., Greve, A. & Downes, D. 1993, AA, 272, 98
Prada, F., Beckman, J. E., McKeith, C. D., Castle, J. & Greve, A. 1994, ApJL, 423, L35

Raychaudhury, S., von Braun, K., Bernstein, G. M. & Guhathakurta, P. 1997, AJ, 113, 2016
Rhee, M. H. 1996, Ph.D. thesis, University of Groningen
Rubin, V. C. & Ford, W. K. 1986, ApJ, 305, 35
Strauss, M. A. & Willick, J. A. 1995, Phys. Rep., 261, 271
Strochi-Bergmann, T. 1991, MNRAS, 249, 404
Tully, R. B. & Fisher, J. R. 1977, AA, 54, 661
Vogt, N. P., Forbes, D. A., Phiillips, A. C., Gronwall, C., Faber, S. M., Illingworth, G. D. & Koo, D. C. 1996, ApJL, 465, L15
Vogt, N. P., Herter, T., Haynes, M. P. & Cpurteau, S. 1993, ApJL, 415, L95
Vogt, N. P., Phiillips, A. C., Faber, S. M., Gallego, J., Gronwall, C., Guzmán, R., Illingworth, G. D., Koo, D. C. & Lowenthal, J. D. 1997, ApJL, 479, L121
Zaritsky, D., Kennicutt, R. C. Jr. & Huchra, J. P. 1994, ApJ, 420, 87